Breakdown of half-metallic ferromagnetism in zinc-blende II-V compounds: First-principles calculations

Yun Li and Jaejun Yu*

Department of Physics and Astronomy, FPRD and Center for Theoretical Physics, Seoul National University, Seoul 151-747, Republic of Korea

(Received 11 July 2008; revised manuscript received 1 September 2008; published 13 October 2008)

We investigated the electronic and magnetic properties of a series of zinc-blend II-V compounds by carrying out density-functional theory calculations including spin-orbit couplings. Contrary to the case of CaN and CaP, the half-metallic characteristics of the II-V compounds such as CaBi were found to be destroyed. Our analysis of the valence-band structures of CaAs, CaSb, and CaBi revealed a critical role of the spin-orbit coupling interactions on the exchange-split band structure, thereby leading to breakdown of the half-metallic ferromagnetism for the systems with heavier group V elements in the zinc-blend II-V compounds.

DOI: 10.1103/PhysRevB.78.165203 PACS number(s): 75.50.Cc, 71.20.Dg, 71.70.Ej

Half-metallic ferromagnets (HMFs), being metallic in only one of the two spin channels, have been considered as an indispensable ingredient in the development of spintronic devices and applications. The realization of the half-metallicity has been investigated extensively since its first prediction on Heusler alloys by de Groot *et al.*[1] However, due to the complexity in their electronic characteristics, manifesting both metallic and insulating properties in a single system at the microscopic level, HMF materials often require complex structures such as ternary spinel, Heusler, and double perovskite structures, also including transition-metal elements as a source of local magnetic moments.

To explore possible spintronics applications of HMFs to semiconductor devices, there have been a great deal of studies exploiting the half metallicity in the binary compounds of zinc-blende (ZB) structure,[2–13] which is simple and compatible with existing III-V and II-VI semiconductors. So far there have been few reports on the fabrication of nanoscale MnAs dots on GaAs, CrSb ultrathin films on the GaSb substrate, and ultrathin CrAs layers in the CrAs/GaAs multilayers.[2–5] In addition, the half-metallic ZB compounds with transition-metal elements were also reported by first-principles density-functional theory (DFT) calculations,[8] whereas a high Curie temperature above 400 K has been observed in experiments for CrAs and CrSb systems.[2,3]

Contrary to the ZB compounds containing transition-metal elements where the localized *d* electrons are responsible for the ferromagnetic component in HMF, several DFT calculations have predicted another kind of ZB II-V compounds as a candidate for the HMFs *without* containing any transition-metal element.[10,12,13] The ZB compounds of alkaline-earth elements Ca, Sr, and Ba combined with all the elements of the group V were shown to be HMFs with a magnetic moment of one Bohr magneton (μ_B) per formula unit cell (f.u.). In these compounds, the presence of a flat *p* band crossing the Fermi level (E_F) in its paramagnetic phase is a key to the half-metallic electronic structure. The narrow *p* band contributes to the exchange energy splitting close to 0.5 eV, consequently leading to an insulating gap in the majority-spin channel and a metallic state in the minority-spin channel.

However, since the *p* states of the heavy elements such as Sb and Bi are affected by the relativistic spin-orbit coupling (SOC), the SOC is expected to play a role in the determination of the II-V valence-band structure consisting of the anion *p* components of As, Sb, and Bi atoms. Therefore, their ground-state electronic and magnetic properties needs to be examined carefully in connection with the half-metallicity of the II-V compounds with heavy group V elements.

In this paper, we report the results of our noncollinear DFT calculations including the spin-orbit coupling terms for the electronic and magnetic properties of the ZB II-V compounds of *AX* (*A*=Ca, Sr, and Ba; *X*=N, P, As, Sb, and Bi). Contrary to the previous reports on the ZB II-V compounds, we found that the ZB II-V compounds containing Sb or Bi are no more half-metallic due to the strong SOC overriding the exchange instability triggered by the flat band feature of the anion *p* states. Our calculations showed a broad spectrum in the physical properties of the ZB II-V compounds, ranging from the half-metallic ferromagnet to an ordinary ferromagnetic metal to a paramagnetic metal. Further analysis of the valence-band structures explains the competition between spin-orbit couplings and exchange interactions as a key ingredient in the determination of ground states of the ZB II-V compounds.

To investigate the role of spin-orbit coupling interactions, we carried out noncollinear DFT calculations including the SOC to determine the electronic structure and magnetic properties of the ZB II-V compounds of *AX* (*A*=Ca, Sr, and Ba; *X*=N, P, As, Sb, and Bi). For the self-consistent electronic structure calculations, we have optimized the equilibrium lattice constant of each *AX* compound under the symmetry constraint of the ZB structure. The structural stability has been extensively examined in the previous works.[12,14] It was discussed that the ZB-type structure of CaAs can exist as a metastable state under certain conditions even though neither ZB nor wurtzite (WZ) structures are the absolute ground state of CaAs. Without further discussions on the stability of the ZB structure, from now on, we like to focus on the electronic and magnetic properties of the II-V compounds at their equilibrium positions within the ZB structure.

The electronic structure calculations were performed by using the OPENMX DFT code,[15] a linear-combination-of-pseudoatomic-orbitals method.[16] The generalized gradient

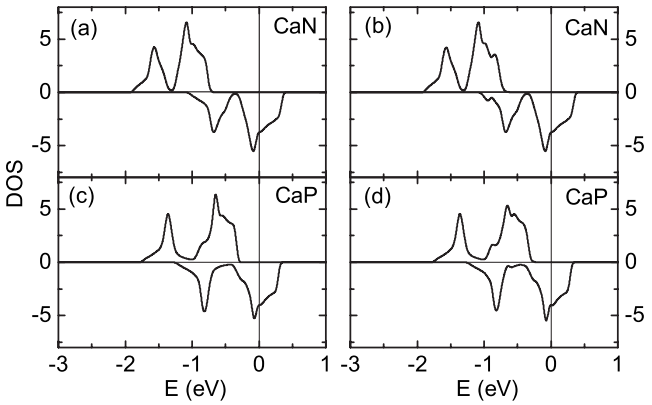

FIG. 1. Total density of states of CaN (a) without and (b) with spin-orbit coupling and CaP (c) without and (d) with spin-orbit coupling, respectively.

approximation (GGA) (Ref. 17) was used for exchange-correlation potential. The effects of spin-orbit couplings via a relativistic j-dependent pseudopotential scheme were included in the noncollinear DFT calculations.[18–20] Double-valence-plus-single-polarization orbitals were taken as a basis set, which were generated with cut-off radii of 6.0, 6.0, and 7.0 a.u. for Ca, Sr, Ba atoms, and 5.0, 5.5, 6.0, 6.5, and 7.0 a.u. for N, P, As, Sb, and Bi atoms, respectively. Troullier-Martins-type pseudopotentials, with a partial core correction for all atoms, were used to replace the deep core potentials by norm-conserving soft potentials in a factorized separable form with multiple projectors. The real-space grid techniques were used with the energy cutoff of 300 Ry in numerical integrations and the solution of the Poisson equation using fast Fourier transformations. For the formula cell containing two atoms, a $(16\times16\times16)$ **k** grid was sampled over the full Brillouin zone. To compare the stability of different magnetic configurations, we calculated total energies of paramagnetic (PM), ferromagnetic (FM), and antiferromagnetic (AFM) configurations in a supercell containing 16 atoms with $(8\times8\times8)$ **k** grid. The total-energy convergence was better than 0.027 meV.

Figure 1 shows the total density of states (DOS) of ZB CaN and CaP with and without SOC. Hereafter we denote the results with and without SOC by using the labels "SOC on" and "SOC off," respectively. The SOC off and SOC on DOSs for both CaN and CaP are almost identical. It is obvious that the SOC effect is negligible for the light elements such as N or P atoms. Consequently the HMF character with a magnetic moment of $1\mu_B$/f.u. remains unchanged regardless of the presence of SOC. In fact, the spin-orbit coupling has virtually no effect on the ZB CaN band structure, as shown in Fig. 2. While the spin-up and spin-down bands are manifest in the collinear, i.e., SOC off band structure of Fig. 2(a), the noncollinear band structure as obtained from the SOC on calculations requires a spin-resolved representation of the bands. In the spin-resolved band plots, as illustrated in Fig. 2(b) and other SOC on band plots in the following figures, we marked each band state by the symbols (△ or ▽), the size of which corresponds to the weight of each spin-component. Figure 2(b) clearly demonstrates that the spin-resolved band structure of CaN with negligible SOC has a

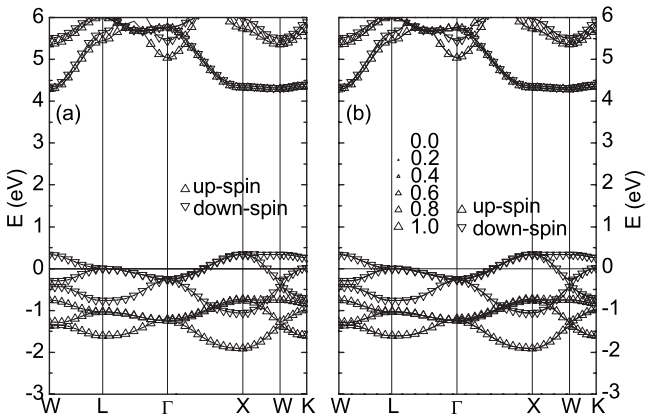

FIG. 2. Band structures of CaN (a) without and (b) with spin-orbit coupling.

clear separation of spin-up and spin-down bands, which is virtually identical to the collinear bands of Fig. 2(a).

To demonstrate the effect of the SOC interactions on the valence-band structures of the ZB II-V compounds, we have calculated the band structures of CaX (X=As, Sb, and Bi) in addition to CaN and CaP. The band plots of CaAs, CaSb, and CaBi are shown in Figs. 3–5, respectively. One of the common features of the SOC off band structures of CaX is a strong exchange-splitting of the flat p bands consisting of the anion p states. The origin of magnetism for the HMF CaX compounds was attributed to the magnetic instability of the narrow p bands at the Fermi level.[12] In fact, the flatness of the p bands are more pronounced in the SOC off band structures of CaX (X=As, Sb, and Bi) than those of CaN and CaP.

The nature of the flat p bands in CaAs has been discussed in the previous work[12] based on the tight-binding model. We can understand the valence-band structure of AX by a simple fcc lattice of anion X (X=N, P, As, Sb, and Bi) with an extraordinarily large lattice constant. In this simplified picture, for instance, the valence-band structure of AX can be mimicked by the partially filled p bands of a fcc Br solid, which features the same p band with the same electron filling as that of AX except the flat bands observed in AX. Indeed, to acquire the flatness, the X p-p hybridization should be counterbalanced by the A d-X p hybridization.

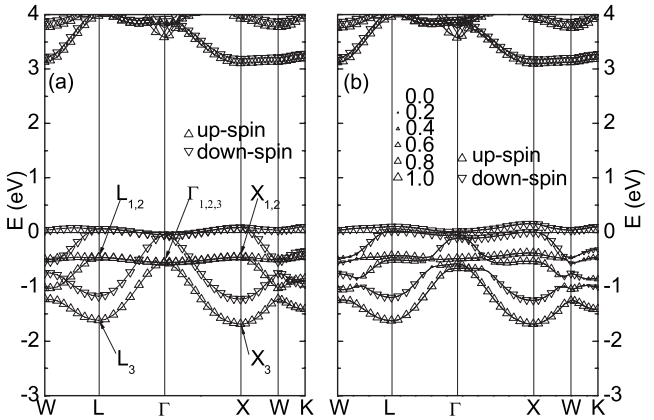

FIG. 3. Band structures of CaAs (a) without and (b) with spin-orbit coupling.

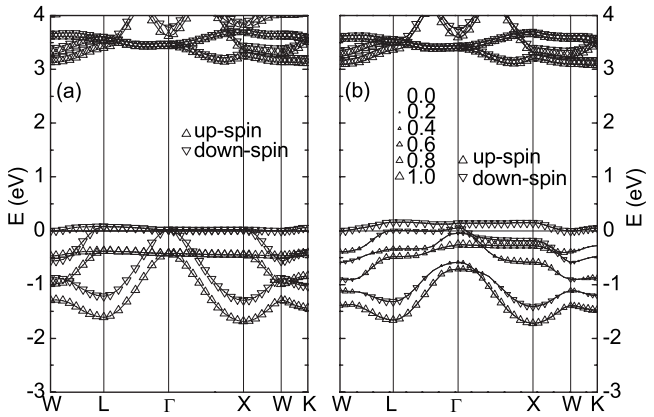

FIG. 4. Band structures of CaSb (a) without and (b) with spin-orbit coupling.

Figure 6 illustrates charge-density profiles of the SOC off spin-up states of CaAs, which are labeled by Γ_i, L_i, and X_i (i=1,2,3) in Fig. 3(a). At the Γ point, the triply degenerate Γ_i (i=1,2,3) states consist of p_x, p_y, and p_z orbitals and form an antibonding configuration among the As p states. Due to the presence of Ca, however, the p-p antibonding states are mixed with the Ca d-As p bonding configurations. Without the Ca d-As p bonding contribution, the energy level of the Γ_i states should have lied at the higher position than those shown in Fig. 3(a). As the **k** vector moves along ΓX and ΓL, the $L_{1,2}$ and $X_{1,2}$ states change into a nonbonding configuration, while the L_3 and X_3 states develop into a strong As p-As p bonding configuration, respectively, as illustrated in Figs. 6(c) and 6(i). Since the nearly flat bands of the doubly degenerate $L_{1,2}$-$\Gamma_{1,2}$-$X_{1,2}$ states contribute to the high DOS at E_F when the SOC is turned off, the Stoner instability would drive the system into the ferromagnetic ground state.

Now let us consider the effect of spin-orbit coupling interactions on the valence-band structure. When SOC is turned on, contrary to the robust HMF band structures of CaN and CaP, the electronic structures of CaX (X=As, Sb, and Bi) change remarkably. Despite that the SOC off valence bands of all the CaX (X=As, Sb, and Bi) compounds are almost identical as shown in Figs. 3–5, the band dispersion and spin characters of the SOC on band structures are mark-

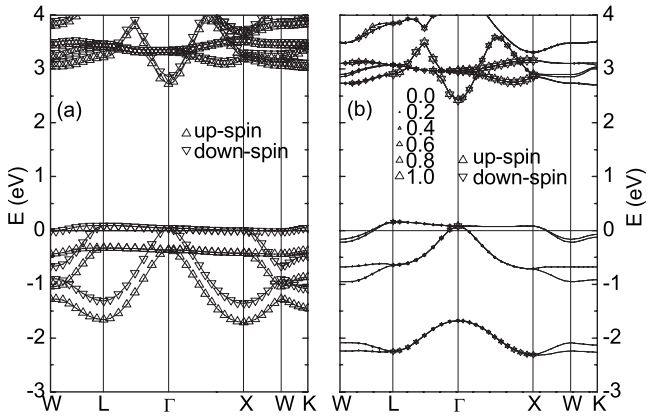

FIG. 5. Band structures of CaBi (a) without and (b) with spin-orbit coupling.

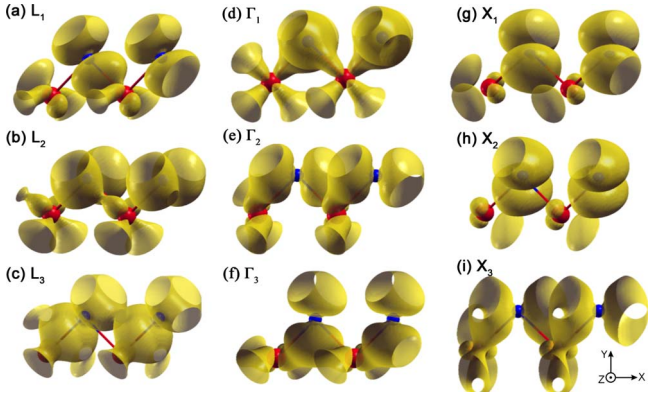

FIG. 6. (Color online) Charge-density profiles of (a) L_1, (b) L_2, (c) L_3, (d) Γ_1, (e) Γ_2, (f) Γ_3, (g) X_1, (h) X_2, and (i) X_3 states of the SOC off CaAs bands, which are labeled in Fig. 3(a). Light (red) spheres represent for Ca atoms and blue (dark) spheres for As atoms.

edly different and evolve as the atomic number of the element X increases from As to Sb to Bi. Since the SOC strength becomes larger for the heavier atoms, the spin-resolved band structures exhibit more complicated features. Before discussing the details of the SOC effects on the spin-resolved band structures, let us examine the evolution of the SOC on DOS of CaX (X=As, Sb, and Bi).

The SOC off DOSs of CaX (X=As, Sb, and Bi) in Figs. 7(a), 7(c), and 7(e) have basically the same characteristics as those of CaN and CaP in Figs. 1(a) and 1(c) except the pronounced flatness in the CaX DOSs. As the SOC strength increases from CaAs to CaSb, the sharp peaks corresponding to the flat p bands broaden and the spin-up and spin-down components seem to smear into each other. [See Fig. 7(d) of CaSb.] For the CaBi case where the SOC energy scale is dominant, the DOS feature shows no spin polarization (SP)

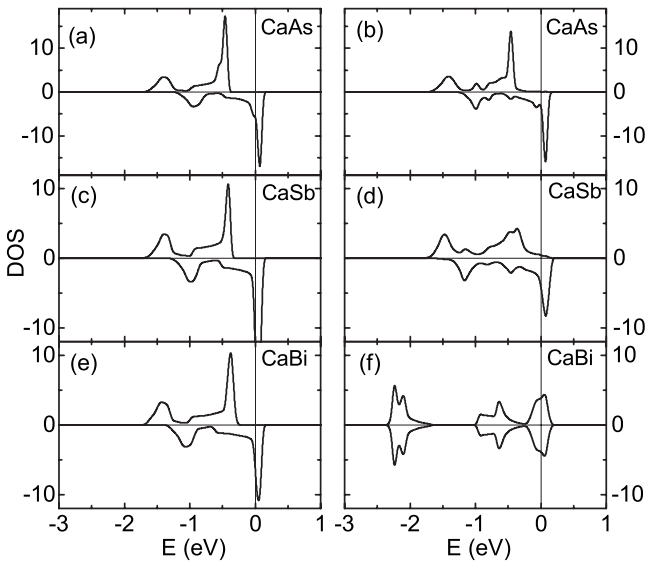

FIG. 7. Total density of states of CaAs (a) without and (b) with spin-orbit coupling, CaSb (c) without and (d) with spin-orbit coupling, and CaBi (e) without and (f) with spin-orbit coupling, respectively.

TABLE I. SP at Fermi level and magnetic moment (M) μ_B/f.u. as obtained from the SOC on calculations.

	N SP/M	P SP/M	As SP/M	Sb SP/M	Bi SP/M
Ca	1.00/1.00	1.00/1.00	0.96/1.10	0.81/1.11	0/0
Sr	1.00/1.00	1.00/1.00	0.97/1.10	0.84/1.17	0/0
Ba	1.00/1.00	1.00/1.00	0.97/1.03	0.79/1.00	0/0

but a clear separation of two peaks: one centered at −2.2 eV corresponding to the $j=1/2$ state and the other at −0.5 eV to $j=3/2$, as shown in Fig. 7(f) of CaBi.

In addition to the evolution of the DOS features, one can observe the change in SP at E_F as well as the magnetic moment (M). The change in SP can be easily understood from the SOC on DOS plots of Fig. 7. The spin polarization of CaAs is close to but not exactly 100%, which means that CaAs is not a HMF in a strict sense, whereas the spin polarization of CaBi is zero. While the half-metallicity in CaAs and CaSb is destroyed moderately, the half-metallic character of CaBi disappears completely.

Table I summarizes the SP at E_F and the magnetic moment (M) of AX (A=Ca, Sr, and Ba; X=N, P, As, Sb, and Bi). Here the SP is defined by the ratio of the spin-up and spin-down DOSs at E_F over the total DOS at E_F. The magnetic moments in Table I include the contribution from both the spin and orbital moments as obtained from the noncollinear calculations. Due to the smearing of the spin-up and spin-down components near E_F, both As and Sb compounds have non-negligible contribution of the majority-spin DOS at E_F. The mixed spin components in the valence bands are clearly shown in the spin-resolved band structures of Figs. 3(b) and 4(b). As the SOC strength increases, some of the noncollinear band states have a strong mixture of spin-up and spin-down components.

Figure 8 shows the effect of SOC on the variation in total energies and magnetic moments of CaAs, CaSb, and CaBi in the ZB structure as a function of lattice constant. Near the equilibrium lattice constant, both CaAs and CaSb show a moderate change in total magnetic moment near $M \approx 1.1$. The variation in M of CaAs and CaSb is attributed to the contribution of the orbital magnetic moment, where the band energies and occupations of the spin-orbit coupled p-states near E_F depends sensitively on the change in lattice constant. The suppression of HMF in CaAs and CaSb for the smaller lattice constant below 6 Å is consistent with the previous work[12] where the lattice constant controls the dispersion of the p band. On the other hand, however, the CaBi system remains nonmagnetic due to the dominance of the SOC interactions.

The SOC on band structures of CaX (X=N, P, As, Sb, and Bi) shown in Figs. 2–5 can be classified into three categories: (i) the CaN-type where the spin-exchange energy of $\Delta E_{ex} \approx 0.5$ eV is dominant, (ii) the CaBi-type where $j=1/2$ and $j=3/2$ bands are well separated by the SOC energy scale of $\Delta E_{so} \approx 2$ eV, and (iii) the CaSb-type, an intermediate case where both ΔE_{ex} and ΔE_{so} compete with each other. In case (i) the CaN-type, the SOC interactions are negligible, i.e., $\Delta E_{ex} \gg \Delta E_{so}$, so that the ferromagnetic band structure is set

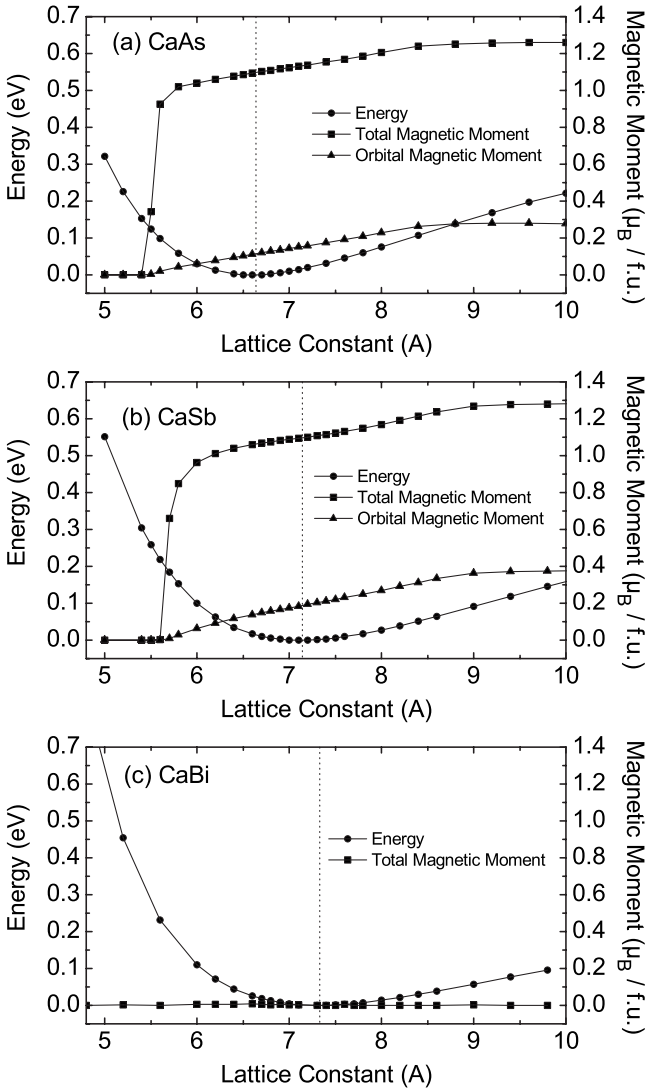

FIG. 8. Total energies and magnetic moments of (a) CaAs, (b) CaSb, and (c) CaBi as a function of lattice constant as calculated with spin-orbit coupling.

by the exchange instability triggered by the narrow p bands. On the other hands, to understand the band structures of types (ii) and (iii), one has to consider both SOC and exchange interactions on the same basis. To estimate the magnitudes of ΔE_{ex} and ΔE_{so}, we calculated the exchange and spin-orbit splitting energies at the Γ point for the SOC off ferromagnetic and SOC on paramagnetic states, respectively. The calculated values of ΔE_{ex} and ΔE_{so} for AX (A=Ca, Sr, and Ba; X=As, Sb, and Bi) are listed in Table II.

For case (ii) the CaBi-type, the SOC energy of ΔE_{so}

TABLE II. Exchange and spin-orbit splitting energies in AX (A=Ca, Sr, and Ba; X=As, Sb, and Bi). Energies are in eV unit.

	As $\Delta E_{ex}/\Delta E_{so}$	Sb $\Delta E_{ex}/\Delta E_{so}$	Bi $\Delta E_{ex}/\Delta E_{so}$
Ca	0.51/0.25	0.44/0.52	0.41/1.88
Sr	0.51/0.23	0.44/0.52	0.41/1.77
Ba	0.48/0.21	0.41/0.47	0.43/1.62

=1.88 eV is much larger than the effective exchange energy of ΔE_{ex}=0.41 eV. Since the SOC term dominates, the valence-band eigenstates of CaBi at the Γ point are well represented by $j=3/2$ and $j=1/2$ states, corresponding to the fourfold and twofold degeneracies, respectively. Even away from the Γ point, the spin-up and spin-down components are mixed up by maintaining its character of the spin-orbit coupled j states. Consequently the average spin polarization in CaBi becomes null so that the ground state is nonmagnetic.

The valence-band structures of CaSb, SrSb, and BaSb are much more complicated as the energy scales of the SOC and exchange interactions become comparable to each other. For example, as listed in Table II, the SOC and exchange energies for CaSb are ΔE_{so}=0.52 eV and ΔE_{ex}=0.44 eV, respectively. The overall shape of the SOC on valence bands of CaSb in Fig. 4(b) resembles those of the SOC off valence bands in Fig. 4(a), whereas the degeneracy of the bands along L-Γ-X is significantly destroyed. Due to the strong contribution of ΔE_{so}, the spin-flip term $(L_+S_-+L_-S_+)$ in the SOC term of $\mathcal{H}_{so}=\lambda_{so}\mathbf{L}\cdot\mathbf{S}$ acts as a perturbation to the exchange-split states.

In conclusion, we have shown that the half-metallic ferromagnetism in ZB II-V compounds weakens significantly for AX (A=Ca, Sr, and Ba; X=As and Sb) and become destroyed completely for ABi (A=Ca, Sr, and Ba) due to the presence of strong spin-orbit coupling interactions. Our noncollinear DFT calculations revealed the evolving features of the spin-orbit coupling and exchange split in the spin-resolved band structures as the atomic number increases from As to Sb to Bi. It is noted that the competition between the spin-orbit coupling and the exchange split is effective only in the ZB II-V compound where the sizable exchange split remains even for the heavy elements such as Sb and Bi due to the "flatness" of p bands. In contrast to the flat p bands of the ZB II-V compounds, the band widths of the flat p bands in the rock-salt structure of CaN, CaSb, and CaBi increase from 1 to 2 eV so that CaSb and CaBi becomes nonmagnetic with no exchange split.[14] Considering the variation in the spin polarizations of ZB II-V compounds, it is suggested that one can control the SOC strength to design either HMF or paramagnetic metal. This SOC-dependent feature may be useful in the spintronics application of HMF materials.

We are grateful to J. I. Lee for helpful suggestions and discussions. This work was supported by the KRF Grant (Grant No. MOEHRD KRF-2005-070-C00041). We also acknowledge the support from KISTI (Korea Institute of Science and Technology Information) under The Supercomputing Application Focus Support Program.

*Corresponding author; jyu@snu.ac.kr

[1] R. A. de Groot, F. M. Mueller, P. G. van Engen, and K. H. J. Buschow, Phys. Rev. Lett. **50**, 2024 (1983).
[2] J. H. Zhao, F. Matsukura, K. Takamura, E. Abe, D. Chiba, and H. Ohno, Appl. Phys. Lett. **79**, 2776 (2001).
[3] H. Akinaga, T. Manago, and M. Shirai, Jpn. J. Appl. Phys., Part 2 **39**, L1118 (2000).
[4] M. Mizuguchi, H. Akinaga, T. Manago, K. Ono, M. Oshima, M. Shirai, M. Yuri, H. J. Lin, H. H. Hsieh, and C. T. Chen, J. Appl. Phys. **91**, 7917 (2002).
[5] K. Ono, J. Okabayashi, M. Mizuguchi, M. Oshima, A. Fujimori, and H. Akinaga, J. Appl. Phys. **91**, 8088 (2002).
[6] Y. Q. Xu, B. G. Liu, and D. G. Pettifor, Phys. Rev. B **66**, 184435 (2002).
[7] W. H. Xie, Y. Q. Xu, B. G. Liu, and D. G. Pettifor, Phys. Rev. Lett. **91**, 037204 (2003).
[8] I. Galanakis and P. Mavropoulos, Phys. Rev. B **67**, 104417 (2003).
[9] B. Sanyal, L. Bergqvist, and O. Eriksson, Phys. Rev. B **68**, 054417 (2003).
[10] K. Kusakabe, M. Geshi, H. Tsukamoto, and N. Suzuki, J. Phys.: Condens. Matter **16**, S5639 (2004).
[11] K. L. Yao, G. Y. Gao, Z. L. Liu, and L. Zhu, Solid State Commun. **133**, 301 (2005).
[12] M. Sieberer, J. Redinger, S. Khmelevskyi, and P. Mohn, Phys. Rev. B **73**, 024404 (2006).
[13] K. L. Yao, J. L. Jiang, Z. L. Liu, and G. Y. Gao, Phys. Lett. A **359**, 326 (2006).
[14] O. Volnianska and P. Bogusławski, Phys. Rev. B **75**, 224418 (2007).
[15] The OPENMX DFT code is available at the web site (http://www.openmx-square.org/) in the constitution of the GNU General Public Licence.
[16] T. Ozaki, Phys. Rev. B **67**, 155108 (2003); T. Ozaki and H. Kino, *ibid.* **69**, 195113 (2004).
[17] J. P. Perdew, K. Burke, and M. Ernzerhof, Phys. Rev. Lett. **77**, 3865 (1996).
[18] A. H. MacDonald and S. H. Vosko, J. Phys. C **12**, 2977 (1979).
[19] G. B. Bachelet, D. R. Hamann, and M. Schluter, Phys. Rev. B **26**, 4199 (1982).
[20] G. Theurich and N. A. Hill, Phys. Rev. B **64**, 073106 (2001).